

# Persulfate activation at cathodic FeN<sub>4</sub> single-atom sites in a sustainable FeNC electrocatalyst for fast degradation of antibiotics in water at near-neutral pH

P. Tirira<sup>a</sup>, S. Mirehbar<sup>b</sup>, S. Fernández-Velayos<sup>b</sup>, P. Herrasti<sup>b</sup>, N. Menéndez<sup>b</sup>, F.J. Recio<sup>b,\*</sup>, I. Sirés<sup>a,\*</sup>

<sup>a</sup> Laboratori d'Electroquímica dels Materials i del Medi Ambient, Departament de Ciència de Materials i Química Física, Secció de Química Física, Facultat de Química, Universitat de Barcelona, Martí i Franquès 1-11, 08028 Barcelona, Spain

<sup>b</sup> Departamento de Química Física Aplicada, Facultad de Ciencias, Universidad Autónoma de Madrid, C/Francisco Tomás y Valiente, 7, Cantoblanco, 28049 Madrid, Spain

## ARTICLE INFO

### Keywords:

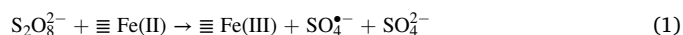
Antibiotic residue  
Electrolytic cell  
Piperacillin  
Single-atom catalyst  
Sulfate radical  
Wastewater treatment

## ABSTRACT

Cathodic persulfate (PS) activation mediated by solid-state Fe(II) produced in situ in a continuous manner has recently emerged as a powerful strategy to degrade organic pollutants. Conversely, the use of single-atom catalysts (SACs) that is now widespread in heterogeneous catalysis for water treatment has never been explored for the design of superior electrocatalysts for PS activation. In this work, the pyrolysis of abundant biopolymer chitosan mixed with an iron salt yielded abundant (15%) single-atom-metal sites (FeN<sub>4</sub>) coordinated with a graphitic matrix. For the first time, PS activation at cathodic Fe<sup>II</sup>-N-C moieties ( $E_{\text{onset}} \sim 0.65$  V/RHE) is demonstrated to be highly effective for the fast degradation of a model antibiotic like piperacillin, being totally removed even in urban wastewater after 90 min at 20 mA cm<sup>-2</sup>.

## 1. Introduction

The advanced oxidation processes (AOPs) based on sulfate radical (SO<sub>4</sub><sup>•-</sup>) have been developed as an alternative to those based on hydroxyl radical (•OH), taking advantage of the longer half-life combined with a high redox potential [1,2]. SO<sub>4</sub><sup>•-</sup> radical can be generated by activation of persulfate (PS), namely peroxymonosulfate (PMS) and peroxydisulfate (PDS), through multiple routes [3]. Among them, the electrochemical activation of PS can be achieved by anodic or cathodic routes. The former has been more widely investigated, focusing on finding high-oxidation-power anodes able to produce •OH as a mediator. Conversely, the cathodic route involves both the classical direct or •H-mediated PS electroreduction and the recently suggested Fe(II)-mediated electroreduction reaction (1) [4].



where  $\equiv$  represents the solid state.

Iron-based nanoparticles have been proven to be good

electrocatalysts for this purpose since the Fe(II) active centers may be continuously regenerated via electron transfer, showing high effectiveness for PS activation during the degradation of organic dyes [4]. Nonetheless, the utilization efficiency of iron sites in nanoparticles is rather low due to their relatively low area-to-volume ratio, thereby wasting most of the catalyst. To overcome this issue, single-atom catalysts (SACs) are now receiving great attention for water treatment [5]. SACs can be prepared by pyrolysis of carbonaceous precursors (e.g., metal-organic frameworks, polymers, biomass). The presence of N in the hydrocarbon backbone facilitates a higher load of metal atoms and their complete dispersion and stabilization [6,7]. The resulting M-N-C moieties (where M preferably accounts for a non-precious metal) have been employed as electrocatalysts, but mainly in the energy field. For example, the oxygen reduction reaction (ORR) [6,8] with such catalysts requires lower reduction overpotentials, thanks to the high electrocatalytic activity of the macrocycles (i.e., MN<sub>4</sub> active sites) present in the resulting graphitized carbon matrix [9]. In contrast, pyrolyzed M-N-C derivatives have not been explored as potential electrocatalysts for PS electroreduction. More specifically, Fe-N-C moieties produced from

\* Corresponding author.

\*\* Corresponding author.

E-mail addresses: [javier.recio@uam.es](mailto:javier.recio@uam.es) (F.J. Recio), [i.sires@ub.edu](mailto:i.sires@ub.edu) (I. Sirés).

abundant biomass might be very appealing because of their non-toxicity and low cost [10].

Antibiotics are nowadays considered one of the most important target organic pollutants in all types of water [11], owing to their impact on superbacteria proliferation. These drugs are highly persistent in the environment, becoming refractory to conventional treatments in municipal facilities [12]. Among them, penicillin- $\beta$ -lactam antibiotics like piperacillin (PIP) are widely administered for bacterial infections, thus being accumulated in water, as observed in Germany [13].

AOPs based on PS are effective in degrading antibiotic residues, and heterogeneous iron-based catalysts suspended in the polluted solutions are excellent activators to trigger the process [1,2,10]. Some SACs have also been tested [7,14], but their performance is still limited because of the gradual oxidation of the metal active sites. Based on this, here we demonstrate the feasibility of Fe–N–C moieties, synthesized from an abundant carbon source like chitosan, to activate the effectively electrocatalytic transformation of PDS into a species with higher oxidation power, as revealed by the fast degradation of the antibiotic PIP.

## 2. Experimental section

### 2.1. Chemicals

Sodium sulfate ( $\text{Na}_2\text{SO}_4$ ), potassium hydroxide (KOH), sodium hydroxide (NaOH), iron(II) sulfate ( $\text{FeSO}_4$ ), and chitosan were purchased from Merck. Piperacillin sodium salt ( $\text{C}_{23}\text{H}_{26}\text{N}_5\text{NaO}_7\text{S}$ ) and Nafion® dispersion (5 wt% in alcohol), as well as methanol ( $\text{CH}_3\text{OH}$ ) and *tert*-butanol ( $\text{C}_4\text{H}_{10}\text{O}$ ), employed as radical scavengers, were acquired from Sigma-Aldrich. Sulfuric acid solution ( $\text{H}_2\text{SO}_4$ , 95–98 %), sodium persulfate ( $\text{Na}_2\text{S}_2\text{O}_8$ , PDS), high purity glacial acetic acid ( $\text{CH}_3\text{COOH}$ ) for High performance liquid chromatography (HPLC), acetonitrile ( $\text{CH}_3\text{CN}$ , UHPLC grade), isopropyl alcohol ( $\text{C}_3\text{H}_7\text{OH}$ ), potassium di-hydrogen phosphate ( $\text{KH}_2\text{PO}_4$ ), and anhydrous sodium hydrogen phosphate ( $\text{Na}_2\text{HPO}_4$ ) were obtained from Panreac. Sodium hypochlorite ( $\text{NaClO}$ ) and *N,N*-diethyl-*p*-phenylenediamine sulfate salt ( $\text{C}_{10}\text{H}_{16}\text{N}_2\cdot\text{H}_2\text{SO}_4$ ) were acquired from Fluka. Ultrapure water was produced on a Millipore Milli-Q system.

### 2.2. Synthesis of the catalyst

Ten gram of chitosan and 10% w/w of  $\text{FeSO}_4$  were added to 50 mL of ultrapure water, and the mixture was stirred for 24 h at room temperature. Subsequently, the mixture was filtered and dried at 80 °C for 12 h. The dry sample was weighted, and 10 mL of 10% w/v KOH solution were added for each 0.4 g of the sample, stirred for 5 h at room temperature, and dried at 80 °C for 12 h. Finally, the precursor was pyrolyzed in a tubular furnace, first at 800 °C for 6 h under  $\text{N}_2$  flow. After this first pyrolysis step, the samples were washed with a 0.5 M  $\text{H}_2\text{SO}_4$  solution at 80 °C for 14 h to leach all the metal ions and the uncoated nanoparticles. Finally, the materials were pyrolyzed at 800 °C for 4 h in an  $\text{N}_2/\text{NH}_3$  atmosphere.

For comparison, an Fe-free catalyst (i.e. N–C sample) was synthesized following the same procedure without adding the  $\text{FeSO}_4$  salt. In addition, C-supported  $\text{Fe}_3\text{O}_4$  nanoparticles were prepared as previously reported [4].

### 2.3. Catalyst analysis

The detailed information is provided in Text S1 of the Supplementary Material.

### 2.4. Degradation tests

The experimental procedures are provided in Text S2 of the Supplementary Material.

## 3. Results and discussion

### 3.1. Catalyst characterization

The different iron species present in the synthesized catalyst were elucidated by Mössbauer spectroscopy. Fig. 1a shows the deconvoluted spectrum of the material, recorded after the double-step pyrolysis process, and Table 1 summarizes the structural parameters of each assigned species.

The assignment reveals the presence of five different iron species, four of which correspond to iron-based particles grown during the pyrolysis processes:  $\alpha$ -Fe,  $\gamma$ -Fe, iron carbides, and iron sulfides. The generation of iron carbides and sulfides results from combining the inorganic iron source with the carbon backbone at high temperatures, resulting in particles covered by a graphitized carbon matrix. In addition, low-spin M–N–C moieties, i.e.,  $\text{FeN}_4/\text{C}$  ( $S = 0$ ) (doublet, D1) sites inserted in the graphitized carbon matrix, are identified in the synthesized catalyst, accounting for 15% of the total iron content. Their presence is expected to favor the massive interaction with PDS and its activation during the degradation trials, in agreement with previous studies that reported the high activity of the Fe–N–C species to promote the ORR and other inner sphere electrocatalytic reactions [6].

To support the formation of  $\text{FeN}_4$  sites, X-ray photoelectron spectroscopy (XPS) analysis of the samples pyrolyzed in the presence and absence of  $\text{FeSO}_4$  was carried out. The full spectra of both samples contain the bands corresponding to O 1s, N 1s, and C 1s, whereas the Fe 2p band is also present in the M–N–C sample (Fig. S1a). The high-resolution spectra of N 1s were fitted to five distinct N-containing groups, whose relative abundance is summarized in Table S1. Both samples exhibited a high percentage of N-pyridinic and N-pyrrolic groups (accounting for more than 55% of N), whereas in the Fe-containing sample, the abundant Fe–N–C moieties (37% of N) confirm that a SAC has been produced.

Fig. 1b shows the voltammogram recorded for the SAC-modified working electrode (i.e., glassy carbon (GC)) in the absence of PDS. Broad peaks related to a clear reversible faradaic process can be observed in the region 0.6–0.7 V vs. RHE (inset figure), which can be associated with the Fe(III)/Fe(II) transition of the  $\text{FeN}_4/\text{C}$  active sites detected by Mössbauer spectroscopy [6]. The catalytic activity of these sites towards the activation of PDS and  $\text{O}_2$  by electron transfer was determined by linear sweep voltammetry (LSV), first for both reactions independently (blue and red curves in Fig. 1b) and then in a mixture of  $\text{PDS} + \text{O}_2$  (pink curve). The PDS and  $\text{O}_2$  electroreduction are triggered at the same potential, showing a similar onset potential ( $E_{\text{onset}}$ ) close to 0.65 V vs. RHE. This phenomenon occurs at a potential very close to the redox potential of the  $\text{FeN}_4/\text{C}$  moieties, which means that these actually behave as active sites for both reactions. Since the electroreduction occurs in the presence of Fe(II), both reactions follow an inner sphere mechanism, with the adsorption of the analyte on the metal sites being the first step. The LSV in the mixed medium confirms this finding, since the  $E_{\text{onset}}$  matches with that of the single tests. This suggests that PDS and  $\text{O}_2$  compete to become activated at the  $\text{FeN}_4/\text{C}$  sites.

It is also important to elucidate the ORR mechanism, since the generation of  $\text{H}_2\text{O}_2$  as a by-product in a  $2\text{e}^- + 2\text{H}^+$  sequence could affect the performance of the PDS-mediated degradation. Indeed,  $\text{H}_2\text{O}_2$  may activate PDS to yield  $\text{SO}_4^{\bullet-}$ , as well as react with Fe(II) to yield  $\bullet\text{OH}$  according to heterogeneous Fenton's reaction [4]. The number of electrons transferred during the ORR has been calculated by the Koutecky-Levich (K-L) equation (see Text S1) in the region under mass transport control (0.2 V vs. RHE) at different rotation rates. Fig. 1c shows that at high overpotential, the total number of electrons (3.8) is close to the theoretical  $4\text{-e}^-$  pathway for  $\text{O}_2$  reduction to  $\text{H}_2\text{O}$ , which allows discarding the production of  $\text{H}_2\text{O}_2$  in this potential range. To verify this finding, the  $\text{H}_2\text{O}_2$  selectivity and the number of electrons were determined from the disk and ring currents obtained with the Rotating ring-disk electrode (RRDE) (equations (S1) and (S2)), as

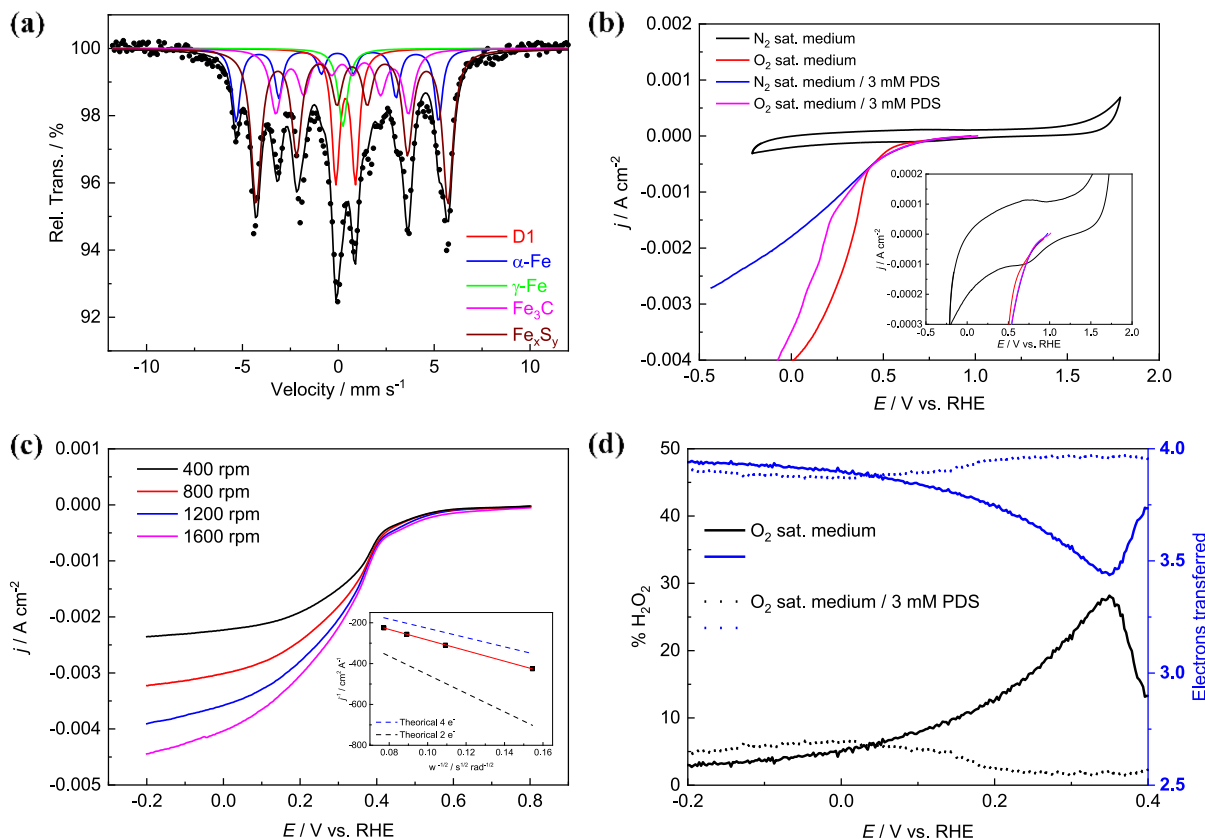


**Fig. 1.** Characterization of the synthesized SAC: **a** room temperature Mössbauer spectrum; **b** cyclic and linear voltammograms under different conditions in a 0.05 M  $\text{Na}_2\text{SO}_4$  solution, registered at the GC disk of an RRDE at  $\omega = 0$  rpm (inset: zoom); **c** polarization curves obtained by LSV with the same RRDE (inset: K-L analysis, see Text S1), in an  $\text{O}_2$ -saturated 0.05 M  $\text{Na}_2\text{SO}_4$  medium without PDS; **d** number of electrons for ORR determined by RRDE (GC disk, Pt ring at  $E = 1.2$  V vs RHE); and  $\text{H}_2\text{O}_2$  selectivity. All voltammograms and polarization curves were recorded at a scan rate ( $v$ ) of  $5 \text{ mV s}^{-1}$ . SAC: single-atom catalyst; GC: glassy carbon; LSV: linear sweep voltammetry; PDS: peroxydisulfate; ORR: oxygen reduction reaction.

**Table 1**

$^{57}\text{Fe}$  Mössbauer analysis parameters of the synthesized single-atom catalyst (SAC): isomer shift (IS), quadrupole splitting (EQ), full width at half maximum (FWHM), hyperfine magnetic field ( $H_{\text{hf}}$ ), and relative spectral area percentage of each component.

Assignment	Signal	IS/ $\text{mm s}^{-1}$	EQ/ $\text{mm s}^{-1}$	FWHM/ $\text{mm s}^{-1}$	$H_{\text{hf}}/\text{T}$	Area/%
D1 $\text{Fe}^{2+}\text{N}_4/\text{C}$ ( $S = 0$ )	Doublet	0.35	1.02	$0.6^a$	–	15
$\gamma\text{-Fe}$	Singlet	0.21	–	$0.6^a$	–	5
$\alpha\text{-Fe}$	Sextet	–0.05	0.02	$0.5^a$	32.7	16
$\text{Fe}_3\text{S}_4$	Sextet	0.71	$0.2^a$	0.64	31.0	44
$\text{Fe}_3\text{C}$	Sextet	0.20	0.0	$0.7^a$	21.4	20

<sup>a</sup> Fixed parameter.

depicted in Fig. 1d. In the absence of PDS, at low overpotentials (0.3–0.4 V vs. RHE), the ORR follows a  $2 \text{ e}^- + 2 \text{ e}^-$  mechanism, with  $\text{H}_2\text{O}_2$  production close to 20% ( $n = 3.5$ ). However, either at high overpotentials (below 0.3 V vs. RHE) or in the presence of PDS, the ORR follows a direct  $4\text{-e}^-$  pathway, which drastically minimizes the role of dissolved  $\text{O}_2$  in the degradation process studied below.

### 3.2. Piperacillin degradation

The removal of PIP was studied in 0.036 mM drug solutions, usually under  $\text{N}_2$  saturation at pH 6.0. Blank experiments in a 0.05 M  $\text{Na}_2\text{SO}_4$  medium are shown in Fig. 2a. PDS alone (1 mM) or in the presence of suspended SAC (50 mg/L) did not cause any noticeable PIP degradation for 120 min, achieving only 5–7% concentration decay. PDS is relatively stable at ambient temperature, and its oxidation power is low [15], while the low SAC content employed (selected to mimic the amount loaded in the cathode in electrochemical tests performed below) is not

able to activate PDS significantly.

Three blank electrochemical assays were then carried out as well in the absence of SAC, using a cell comprising a Pt anode and an unmodified or modified GC cathode at a current density ( $j$ ) of  $20 \text{ mA cm}^{-2}$ . Fig. 2b shows the evolution of PIP concentration over time in electro-oxidation (EO) treatments in an  $\text{N}_2$ -saturated 0.05 M  $\text{Na}_2\text{SO}_4 + 1 \text{ mM}$  PDS solution. The use of unmodified GC only led to 25% degradation at 120 min. The modification of GC with chitosan-derived carbon particles did not enhance the PIP removal, obtaining a very similar concentration decay profile. This means that such carbon is not a good PDS activator, and the contribution of the adsorption process in subsequent trials can be neglected as well. Fig. 2b also depicts the enhanced but still slow and partial PIP concentration decay (58% after 120 min) when GC was coated with C-supported  $\text{Fe}_3\text{O}_4$  nanoparticles, synthesized as in previous research [4], thus requiring a better catalyst.

Fig. 2c presents the electrochemical tests performed with a SAC-modified GC cathode. In the EO process at  $j$  of  $10 \text{ mA cm}^{-2}$  in the

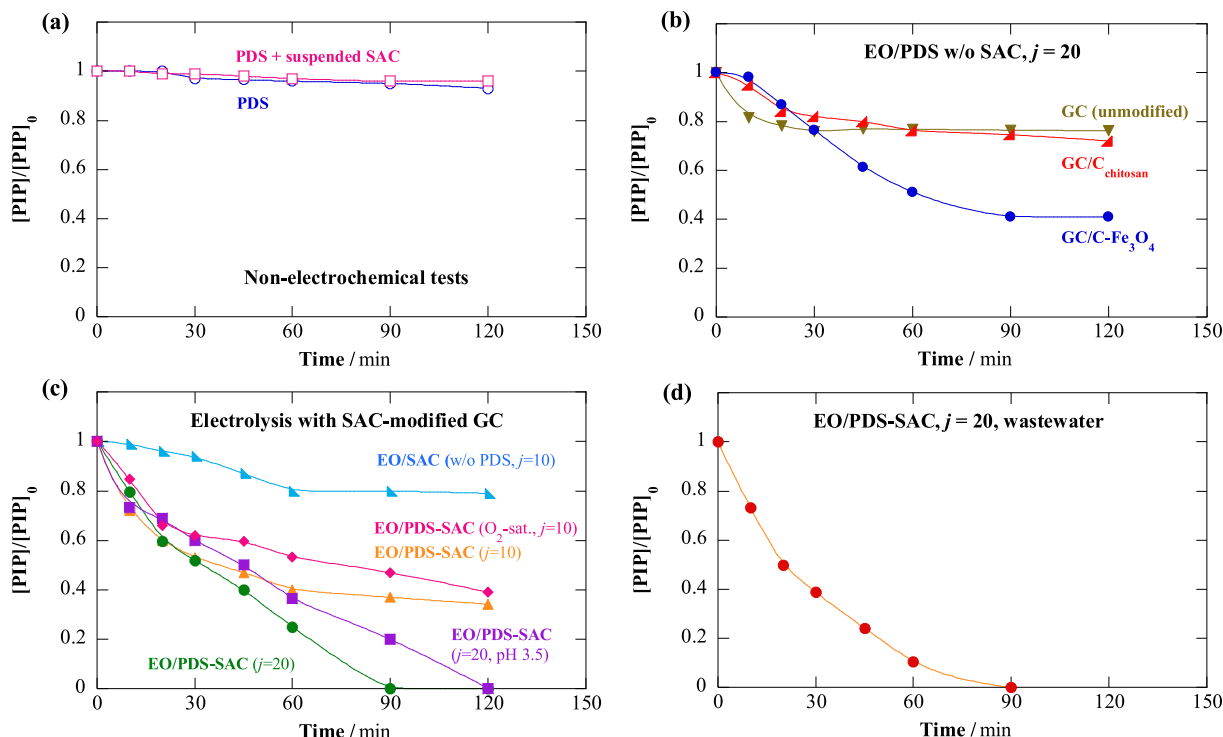
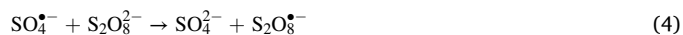


**Fig. 2.** Normalized PIP concentration decays during the treatment of 0.036 mM PIP solutions (always with N<sub>2</sub>-saturated medium at pH 6.0, unless stated otherwise): **a** blank test in 0.05 M Na<sub>2</sub>SO<sub>4</sub> medium; **b** different electrochemical trials in 0.05 M Na<sub>2</sub>SO<sub>4</sub> medium at 20 mA cm<sup>-2</sup>, using a modified or unmodified GC as the cathode; **c** similar tests, but using a SAC-modified GC, at 10 or 20 mA cm<sup>-2</sup>; **d** PIP removal in actual wastewater under the best degradation conditions. PDS always has a concentration of 1 mM. PIP: piperacillin; GC: glassy carbon; SAC: single-atom catalysts; PDS: peroxydisulfate.

absence of PDS, only 21% degradation was achieved, which can be explained by the low oxidation power of the Pt anode that is unable to produce a high concentration of adsorbed <sup>•</sup>OH. All subsequent electrolytic trials were made with 1 mM PDS, evidencing the activation of PDS in all cases. At  $j = 10$  mA cm<sup>-2</sup>, 61% and 65% removals were achieved at 120 min in O<sub>2</sub>- and N<sub>2</sub>-saturated Na<sub>2</sub>SO<sub>4</sub> medium, respectively. The slower abatement in the presence of O<sub>2</sub> can be attributed to the competing adsorption in some of the FeN<sub>4</sub>/C active sites, as mentioned above.

The fastest removal of PIP in Na<sub>2</sub>SO<sub>4</sub> medium was attained after 90 min at 20 mA cm<sup>-2</sup> and pH 6, being slightly decelerated at pH 3.5 with total disappearance at 120 min. Moreover, at 90 min, the leached iron at pH 6.0 determined by Inductively coupled plasma mass spectrometry (ICP-MS) was below 40 ppb. Considering the poor oxidation power of the Pt anode, the enhancement upon  $j$  increase can be explained by the quicker PDS activation. In turn, the resulting active species can yield <sup>•</sup>OH from reaction (2) [4]. Note that although SO<sub>4</sub><sup>•-</sup> formed from reaction (1) is suggested to be the main active species, the M–N–C SACs have been recently manifested to be effective for the activation of PS via a non-radical pathway [16]. To gain further insight into the oxidation mechanism, the optimal degradation trial (i.e., EO/PDS-SAC, at  $j$  of 20 mA cm<sup>-2</sup> and pH 6), was repeated in the presence of radical scavengers, as described by some authors [17,18]. Fig. S2 confirms that SO<sub>4</sub><sup>•-</sup> is the main reactive oxygen species when using M–N–C catalyst, with a direct (30%) or indirect (i.e., <sup>•</sup>OH production via reaction (2), 45%) contribution. Hence, 25% of degradation could be explained by the action of O<sub>2</sub><sup>•-</sup>/<sup>1</sup>O<sub>2</sub> and/or non-radical mechanisms.

The slower PIP degradation at an acidic pH agrees with the decline observed by other authors. This has been associated with an excess of sulfate radicals produced, which promote parasitic reactions (3) and (4) [19].



Aiming to corroborate the good results, the viability of the SAC-mediated PDS activation was evaluated in urban wastewater with the spiked drug. Usually, the oxidation efficiency of a radical-based AOP system decreases due to the scavenging effect of background inorganic anions and natural organic matter. Nonetheless, Fig. 2d illustrates the high effectiveness of the system under study, with even faster PIP removal as compared to the same trial in Na<sub>2</sub>SO<sub>4</sub> solution (Fig. 2c).

Complete disappearance occurred at 90 min, following a quicker decay kinetics. Such excellent performance can then be attributed to: (i) the production of active chlorine (and chlorine radicals) upon oxidation of Cl<sup>-</sup> by activated PDS [20]. This was verified by detecting chlorine during the electrolysis of a 10 mM NaCl solution at 20 mA cm<sup>-2</sup>; and/or (ii) the aforementioned nonradical oxidation pathway attributed to the M–N–C catalyst, which is less susceptible to parasitic reactions typically found in a complex water matrix.

#### 4. Conclusion

To summarize, a powerful strategy for persulfate (PS) activation using abundant biomass waste has been developed, based on cathodic single-atom catalyst (SAC), overcoming the inefficiency of nanoparticle electrocatalysts and suspended SACs. The excellent performance even in actual wastewater opens the door to design SACs based on other MN<sub>4</sub> sites that might allow decoupling the PS activation from 4-e<sup>-</sup> oxygen reduction reaction (ORR), eventually boosting the degradation of the organic pollutants.

#### CRedit author statement

**Paola Tirira:** Methodology, Data curation, Writing-original draft. **Seyedkeyvan Mirehbar:** Methodology. **Sergio Fernández-Velayos:**

**Methodology.** **Pilar Herrasti:** Funding acquisition, Supervision. **Nieves Menéndez:** Methodology. **Francisco Javier Recio:** Data curation, Formal analysis, Writing-original draft, Writing-review & editing. **Ignasi Sirés:** Data curation, Formal analysis, Funding acquisition, Writing-original draft, Writing-review & editing.

### Declaration of competing interest

The authors declare that they have no known competing financial interests or personal relationships that could have appeared to influence the work reported in this paper.

### Data availability

Data will be made available on request.

### Acknowledgments

The authors are grateful to projects PID2019-109291RB-I00, PID2021-123431OB-I00, PID2022-140378OB-I00 and PDC2022-133624-I00 (MCIN/AEI/10.13039/501100011033, Spain), as well as to 2021PROD00171 (AGAUR, Spain). P.T. acknowledges her FPI PhD scholarship (PRE2020-095114, MICINN, Spain), co-financed by ESF. We also thank the valuable support from Mr. L. Zhao with XPS analysis.

### Appendix A. Supplementary data

Supplementary data to this article can be found online at <https://doi.org/10.1016/j.mtsust.2023.100581>.

### References

- [1] S. Cai, Y. Liu, J. Chen, FeCu-biochar enhances the removal of antibacterial sulfapyridine from groundwater by activation of persulfate, *Environ. Chem. Lett.* 18 (5) (2020) 1693–1700, <https://doi.org/10.1007/s10311-020-01026-5>.
- [2] P. Xia, C. Wang, Q. He, Z. Ye, I. Sirés, MOF-derived single-atom catalysts: the next frontier in advanced oxidation for water treatment, *Chem. Eng. J.* 452 (2023), 139446, <https://doi.org/10.1016/j.cej.2022.139446>.
- [3] Y. Gao, Q. Wang, G. Ji, A. Li, Degradation of antibiotic pollutants by persulfate activated with various carbon materials, *Chem. Eng. J.* 429 (2022), 132387, <https://doi.org/10.1016/j.cej.2021.132387>.
- [4] S. Mirehbar, S. Fernández-Velayos, E. Mazario, N. Menéndez, P. Herrasti, F. J. Recio, I. Sirés, Evidence of cathodic peroxydisulfate activation via electrochemical reduction at Fe(II) sites of magnetite-decorated porous carbon: application to dye degradation in water, *J. Electroanal. Chem.* 902 (2021), 115807, <https://doi.org/10.1016/j.jelechem.2021.115807>.
- [5] P. Xia, Z. Ye, L. Zhao, Q. Xue, S. Lanzaalaco, Q. He, X. Qi, I. Sirés, Tailoring single-atom FeN<sub>4</sub> moieties as a robust heterogeneous catalyst for high-performance electro-Fenton treatment of organic pollutants, *Appl. Catal. B Environ.* 322 (2023), 122116, <https://doi.org/10.1016/j.apcatb.2022.122116>.
- [6] R. Venegas, K. Muñoz-Becerra, C. Candia-Onfray, J.F. Marco, J.H. Zagal, F.J. Recio, Experimental reactivity descriptors of M-N-C catalysts for the oxygen reduction reaction, *Electrochim. Acta* 332 (2020), 135340, <https://doi.org/10.1016/j.electacta.2019.135340>.
- [7] Y. Liu, H. Zhao, Persulfate activation by single-atom catalysts for the removal of organic pollutants: a review, *Resour. Chem. Mat.* 2 (2023) 63–79, <https://doi.org/10.1016/j.recmm.2022.09.002>.
- [8] K. Muñoz-Becerra, R. Venegas, L. Duque, J.H. Zagal, F.J. Recio, Recent advances of Fe–N–C pyrolyzed catalysts for the oxygen reduction reaction, *Curr. Opin. Electrochem.* 23 (2020) 154–161, <https://doi.org/10.1016/j.coelec.2020.08.006>.
- [9] Y. Wang, H. Su, Y. He, L. Li, S. Zhu, H. Shen, P. Xie, X. Fu, G. Zhou, C. Feng, D. Zhao, F. Xiao, X. Zhu, Y. Zeng, M. Shao, S. Chen, G. Wu, J. Zeng, C. Wang, Advanced electrocatalysts with single-metal-atom active sites, *Chem. Rev.* 120 (21) (2020) 12217–12314, <https://doi.org/10.1021/acs.chemrev.0c00594>.
- [10] W. Sang, X. Xu, C. Zhan, W. Lu, D. Jia, C. Wang, Q. Zhang, F. Gan, M. Li, Recent advances of antibiotics degradation in different environment by iron-based catalysts activated persulfate: a review, *J. Water Process Eng.* 49 (2022) 103075, <https://doi.org/10.1016/j.jwpe.2022.103075>.
- [11] Q. Yuan, S. Qu, R. Li, Z.-Y. Huo, Y. Gao, Y. Luo, Degradation of antibiotics by electrochemical advanced oxidation processes (EAOPs): performance, mechanisms, and perspectives, *Sci. Total Environ.* 856 (2023), 159092, <https://doi.org/10.1016/j.scitotenv.2022.159092>.
- [12] T.D. Nguyen, T. Lee, T.V. Tran, V.H. Nguyen, Multicomponent photocatalysts for synergic removal of antibiotics in aqueous media: a review, *Environ. Chem. Lett.* 21 (2023) 935–980, <https://doi.org/10.1007/s10311-022-01533-7>.
- [13] A. Timm, E. Borowska, M. Majewsky, S. Merel, C. Zwiener, S. Bräse, H. Horn, Photolysis of four  $\beta$ -lactam antibiotics under simulated environmental conditions: degradation, transformation products and antibacterial activity, *Sci. Total Environ.* 651 (2019) 1605–1612, <https://doi.org/10.1016/j.scitotenv.2018.09.248>.
- [14] D. Yang, Y. Hu, P. Hong, G. Shen, Y. Li, J. He, K. Zhang, Z. Wu, C. Xie, J. Liu, L. Kong, Preassembly strategy to anchor single atoms on carbon nitride layers achieving versatile Fenton-like catalysis, *Sep. Purif. Technol.* 308 (2023), 122955, <https://doi.org/10.1016/j.seppur.2022.122955>.
- [15] L. Xiong, W. Ren, H. Lin, H. Zhang, Efficient removal of bisphenol A with activation of peroxydisulfate via electrochemically assisted Fe(III)-nitrotriacetic acid system under neutral condition, *J. Hazard Mater.* 403 (2021), 123874, <https://doi.org/10.1016/j.jhazmat.2020.123874>.
- [16] T. Yang, S. Fan, Y. Li, Q. Zhou, Fe–N/C single-atom catalysts with high density of Fe–N<sub>x</sub> sites toward peroxydisulfate activation for high-efficient oxidation of bisphenol A: electron-transfer mechanism, *Chem. Eng. J.* 419 (2021), 129590, <https://doi.org/10.1016/j.cej.2021.129590>.
- [17] A.J. dos Santos, I. Sirés, E. Brillas, Removal of bisphenol A from acidic sulfate medium and urban wastewater using persulfate activated with electrogenerated Fe<sup>2+</sup>, *Chemosphere* 263 (2021), 128271, <https://doi.org/10.1016/j.chemosphere.2020.128271>.
- [18] N. Du, Y. Liu, Q. Li, W. Miao, D. Wang, S. Mao, Peroxydisulfate activation by atomically-dispersed Fe–N<sub>x</sub> on N-doped carbon: mechanism of singlet oxygen evolution for nonradical degradation of aqueous contaminants, *Chem. Eng. J.* 413 (2021), 127545, <https://doi.org/10.1016/j.cej.2020.127545>.
- [19] C. Liang, Z.-S. Wang, C.J. Bruell, Influence of pH on persulfate oxidation of TCE at ambient temperatures, *Chemosphere* 66 (2007) 106–113, <https://doi.org/10.1016/j.chemosphere.2006.05.026>.
- [20] J. Lee, U. Von Gunten, J.-H. Kim, Persulfate-based advanced oxidation: critical assessment of opportunities and roadblocks, *Environ. Sci. Technol.* 54 (6) (2020) 3064–3081, <https://doi.org/10.1021/acs.est.9b07082>.